JTTEE5 17:838–845
DOI: 10.1007/s11666-008-9223-z
1059-9630/$19.00 © ASM International

Peer Reviewed

Thermal Failure of Nanostructured Thermal Barrier Coatings with Cold-Sprayed Nanostructured NiCrAlY Bond Coat

Qiang Zhang, Chang-Jiu Li, Yong Li, Shao-Ling Zhang, Xiu-Ru Wang, Guan-Jun Yang, and Cheng-Xin Li

(Submitted May 13, 2008; in revised form August 9, 2008)

Nanostructured thermal barrier coatings (TBCs) were deposited by plasma spraying using agglomerated nanostructured YSZ powder on Inconel 738 substrate with cold-sprayed nanostructured NiCrAlY powder as bond coat. The isothermal oxidation and thermal cycling tests were applied to examine failure modes of plasma-sprayed nanostructured TBCs. For comparison, the TBC consisting of conventional microstructure YSZ and conventional NiCrAlY bond coat was also deposited and subjected to the thermal shock test. The results showed that nanostructured YSZ coating contained two kinds of microstructures; nanosized zirconia particles embedded in the matrix and microcolumnar grain structures of zirconia similar to those of conventional YSZ. Although, after thermal cyclic test, a continuous, uniform thermally grown oxide (TGO) was formed, cracks were observed at the interface between TGO/BC or TGO/YSZ after thermal cyclic test. However, the failure of nanostructured and conventional TBCs mainly occurred through spalling of YSZ. Compared with conventional TBCs, nanostructured TBCs exhibited better thermal shock resistance.

Keywords bond coat, cold spraying, nanostructure, plasma spraying, thermal barrier coating, YSZ

1. Introduction

Thermal barrier coatings (TBCs) are favorably used as protective coatings on hot section components in advanced gas turbine engines to withstand increased inlet temperatures and thus improving engine performance (Ref 1, 2). Failure of a TBC system is often associated with the formation of a thermally grown oxide (TGO) layer resulting in Al depletion in the bond coat. It has been shown that failure of plasma-sprayed TBCs often occurs through spalling of the ceramic layer near the ceramic/bond coat interface but mostly within the ceramic layer (Ref 3-5).

This article is an invited paper selected from presentations at the 2008 International Thermal Spray Conference and has been expanded from the original presentation. It is simultaneously published in *Thermal Spray Crossing Borders, Proceedings of the 2008 International Thermal Spray Conference*, Maastricht, The Netherlands, June 2-4, 2008, Basil R. Marple, Margaret M. Hyland, Yuk-Chiu Lau, Chang-Jiu Li, Rogerio S. Lima, and Ghislain Montavon, Ed., ASM International, Materials Park, OH, 2008.

Qiang Zhang, Chang-Jiu Li, Yong Li, Shao-Ling Zhang, Xiu-Ru Wang, Guan-Jun Yang, and **Cheng-Xin Li**, State Key Laboratory for Mechanical Behavior of Materials, School of Materials Science and Engineering, Xi'an Jiaotong University, Xi'an, Shaanxi 710049, P.R. China. Contact e-mail: licj@mail.xjtu.edu.cn.

Recently, nanostructured coatings have received wide interest because of their extraordinary properties including hardness, strength, ductility, and toughness. Accordingly, nanostructured materials are expected to be applied to advanced thermal barrier coatings. In the last decade, several papers (Ref 6-12) have dedicated to systematic study of nanostructured materials in the area of surfaces and coatings, including thermal spray coatings.

One of the biggest challenges in thermal spraying nanomaterials is to retain the nanostructure of the feedstock to deposit. If nanostructured powder particles are completely melted during spraying, the traditional behavior of thermal spray particles, such as solidification, nucleation, and growth, will take place. Such processes will destroy the original nanostructured features of the feedstock. During plasma spraying of nanostructured ceramics it is necessary to partially melt the powder particles to achieve the necessary physical conditions for cohesion and adhesion. Therefore, a bimodal microstructure will be present in the deposited coating. The low elastic properties of nanostructured YSZ fraction may benefit from the tolerance of TBCs to the thermal strain (Ref 8). However, the performance of a superior TBC is greatly associated with the features of the bond coat underlying YSZ topcoat. In a previous study (Ref 10), it was found that a uniform oxide can be formed on a cold-sprayed nanostructured NiCrAlY coating surface.

In this study, the nanostructured YSZ and conventional YSZ were deposited on a cold-sprayed nanostructured NiCrAlY bond coat and a conventional NiCrAlY bond coat, respectively. The failure behavior of the plasma-sprayed nanostructured TBCs was investigated in comparison with that of the conventional TBCs. The features

of TGO and cracking in the vicinity of TGO during thermal cyclic test were examined.

2. Experimental Materials and Procedures

The conventional and nanostructured Ni-20Cr-10Al-1Y and ZrO_2-$8Y_2O_3$ powder were used to deposit the bond coat and the ceramic coat, respectively. The nanostructured NiCrAlY powder was produced by the mechanical milling process in a planetary ball miller (ND6-2L, Nanjing University Tianzun Electron Co. Ltd., Nanjing, China) using conventional Ni-20Cr-10Al-1Y powder (KF-343, BGRIMM, Beijing, China). The mean particle size of the nanostructured and conventional NiCrAlY powder were 37 and 23 μm determined by laser size measurement (MASTERSIZER 2000, Malvern Instruments Ltd., UK), respectively. The oxygen contents of the conventional NiCrAlY powders, nanostructured NiCrAlY powders, and as-sprayed NiCrAlY bond coat were determined using an oxygen determinator (RO-316, LECO, USA). The oxygen contents of the conventional and nanostructured NiCrAlY powders were 0.028 and 0.75 wt.%, respectively. The particle size of the agglomerated nanostructured YSZ (DiDa Nano-Materials Co. Ltd., Hubei, China) is nominally from 40 to 90 μm, and the particle size of the conventional YSZ (XianDao Plasma Materials Co. Ltd., YiYang, China) is from 30 to 45 μm. An IN738 superalloy was used as a substrate.

The nanostructured and conventional bond coating in a thickness of 100-150 μm was deposited on the IN738 substrate by cold spraying (CS) using a homemade system (Ref 13). Helium was used as accelerating gas, operating at a pressure of 2.5 MPa. The spray nozzle has a circular shape with a throat diameter of 2 mm and exit diameter of 6 mm. The nanostructured and conventional YSZ of 200-250 μm thick was deposited on the nanostructured and conventional NiCrAlY bond coat, respectively, by air plasma spraying (APS) using a commercial plasma spray system (GDP-K, Jiujiang, 80 kW class). Argon was used as the primary plasma operating gas and hydrogen was used as an auxiliary gas. The pressures of argon and hydrogen were operated at 0.7 and 0.5 MPa, respectively. The flow rate of argon and hydrogen was fixed to 33 and 2 L/min, respectively. Nitrogen was used as powder feed gas. Plasma jet was operated to deposit the coating at the power of 40 kW.

Crystalline structure of YSZ powder and coating was characterized by X-ray diffraction diffractometer (XRD-6000, Shimadzu, Kyoto, Japan) using Cu-Kα radiation. The mean grain size of YSZ powders was calculated using the Scherrer equation (Ref 9). The average grain size of the YSZ powder was approximately 36 nm.

Figure 1 shows morphology of the nanostructured YSZ powder. Clearly, powder particles are spherical (Fig. 1a). The examination of the fractured particle cross-section at a high magnification suggests that the particle is porous (Fig. 1b). The grain size of the nanostructured NiCrAlY coating was reported elsewhere (Ref 13). The estimation yielded a grain size ranging from 15 to 50 nm.

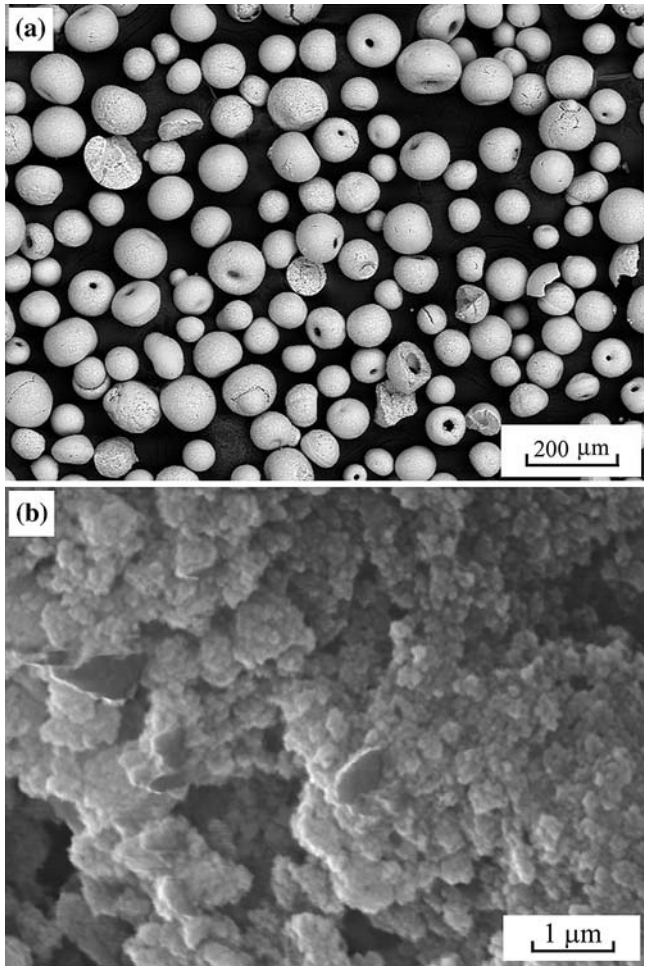

Fig. 1 General surface morphology (a) and the morphology (b) of the fractured nanostructured YSZ powder

The surface layer of the deposited nanostructured bond coat was densified through shot-peening treatment. Subsequently, the bare bond coatings were heat treated at a temperature of 1000 °C for 4 h in an argon atmosphere prior to YSZ deposition. The thermal cyclic test of TBCs samples consisted of a 2 min oven-preheated heating at 1000 °C, 1000 °C × 27 min holding and cooling down to room temperature in 3 min by a forced air cooling in each cycle. To speed up the thermal cyclic test, after 300 cycles at a furnace temperature of 1000 °C, the same thermal cyclic test was continued except that the holding temperature was raised to 1150 °C. Isothermal oxidation test was carried out under a temperature of 1000 °C. The coating microstructure and compositions were characterized using a scanning electron microscope (SEM, VEGA II-XMU, TESCAN, Czech) with an energy dispersive spectrometer (EDS) through the cross-section. The TGO thickness was measured from the SEM micrographs. TGO thickness measurements were made at different positions for 30 times using three SEM micrographs along the interface between YSZ and the bond coat.

3. Results and Discussion

3.1 Microstructure of the As-Sprayed Nanostructured TBC

Figure 2(a) shows the microstructure of the TBC consisting of the as-sprayed nanostructured YSZ. It can be noted in Fig. 2(b) that two types of microstructure are present in the nanostructured YSZ coating: columnar grains solidified from the melted fraction of YSZ powder and the loose microstructure retained from the unmelted YSZ powder. Therefore, YSZ coating exhibits a bimodal microstructure consisting of nanosized particles retained from the powder and microcolumnar grains formed through the solidification of the melted fraction in spray particles. The porous structures will enhance the thermal insulation effect of TBCs (Ref 6-12, 14-16). The coating porosity depends on the melting degree of powder particles during deposition. The as-sprayed bond coat was compacted and oxides were not present in the bond coat, as shown inn Fig. 2(c) and (e), although some pores were present in the nanostructured bond coating. The oxygen contents of the nanostructured and conventional bond coats were 0.72 and 0.024 wt.%, respectively, which were similar to those of the nanostructured and conventional powders. This fact indicates that the in-flight particles are subjected to little oxidation. It can be observed from Fig. 2(a), (d), and (f) that a uniform and exclusive oxide layer was formed at the interface between the YSZ and bond coating. The average thickness of oxides on the nanostructured and conventional bond coats was 1.1 ± 0.3 and 0.7 ± 0.1 μm, respectively. EDS analysis shows that the coating surface layer is rich in Al and O. This fact indicates that a dense Al_2O_3 was preferably nucleated during the heat treatment in argon atmosphere of both nanostructured NiCrAlY and conventional NiCrAlY coatings prior to YSZ deposition. Moreover, the oxide scale formed on the nanostructured NiCrAlY bond coat was denser than that on the conventional NiCrAlY bond coat. This fact implies that the uniform oxide film on the nanostructured NiCrAlY coating surface grew very rapidly during the initial stage of oxidation. This may be attributed to the nanostructure features of the nanostructured NiCrAlY coating. The small grains promote fast diffusion of elemental Al toward the surface, to provide a sufficient Al source for Al_2O_3 growth (Ref 17-19).

3.2 Microstructure of TGO Formed by Isothermal Oxidation of TBC

The typical microstructure of the nanostructured TBC sample and conventional sample isothermally oxidized for 100 h at 1000 °C are shown in Fig. 3(a) and (b). The average thickness of the oxide layer on the nanostructured and conventional bond coat, measured on polished cross-sections, was approximately 2.2 ± 0.3 and 2.0 ± 0.4 μm, respectively. It can be seen in Fig. 3(a) and (b) that the oxide layer on the bond coatings was uniform and continuous. EDS analysis shows that the oxide film mainly is composed of Al and O elements, indicating the formation of Al_2O_3. In addition, the adhesion of the bond coating to YSZ coating is enhanced by forming an exclusive α-Al_2O_3 scale at the interface between the bond coat and YSZ. No cracks were observed in the vicinity of the TGO.

3.3 Cracking of the TBCs During Thermal Cycling Test at 1000 °C

Figure 4 shows a typical cross-sectional view of a nanostructured TBC specimen after 300 times thermal cycles at the holding temperature of 1000 °C. The YSZ coating was intact after the test. A highly undulated bond coat/TGO interface was observed. These undulations are due to the deliberate roughening of the bond coat surface prior to topcoat deposition for improving the topcoat adhesion by mechanical keying. However, these undulations may give rise to an out-of-plane tension, which is primarily responsible for the ultimate failure of TBCs (Ref 1, 2).

It is worth noting in Fig. 5 that the TGO formed at the interface between the top YSZ coat and the bond coat exhibits a uniform morphology along the interface, which depends evidently on the surface morphology of the as-deposited bond coat. Microstructural observations showed cracks in the vicinity of the TGO. Cracking occurred within the topcoat at the interface between TGO and YSZ or near the crest of the bond coat undulations. The linkage of such cracks through propagation likely results in the ultimate failure of the TBC. Crack was also present at the interface between TGO and bond coat, where the TGO is thick, which is possibly due to thermal expansion mismatching, as shown in Fig. 6(a) and (b). It can be observed from the higher magnification view of the bond coat undulation crest in Fig. 6 that the separation occurred between the bond coat and the TGO at the crest or between the TGO and the topcoat. Crack also runs across the TGO. These features were commonly observed around the undulations in these TBCs. However, in local domains cracking also occurred within the topcoat and no crack was presented at the interface of the TGO/YSZ. This fact suggests that the nanostructured YSZ exhibits a high strain tolerability.

3.4 Failure Mode After Thermal Cycling at 1150 °C

Table 1 shows thermal cyclic life of two different TBCs under different thermal cyclings. It was found that the number of thermal shock cycles to failure at 1150 °C of the nanostructured TBCs was about two to four times larger than the conventional TBCs after the thermal cyclic test for 300 cycles at 1000 °C, and exhibited a little increase after the isothermal oxidation for 100 h at 1000 °C. These facts indicate that the influence of the low-temperature thermal cycling on the thermal cyclic lifetime is larger for the conventional TBCs than the nanostructured TBCs.

Figure 7 shows the cross-sectional micrograph of the failed nanostructured TBCs subjected to thermal cyclic test at 1150 °C. The sample shown in Fig. 7(a) has experienced thermal cyclic test for 300 cycles at 1000 °C before the thermal cyclic test at 1150 °C, while the sample in Fig. 7(b) experienced the isothermal oxidation test at

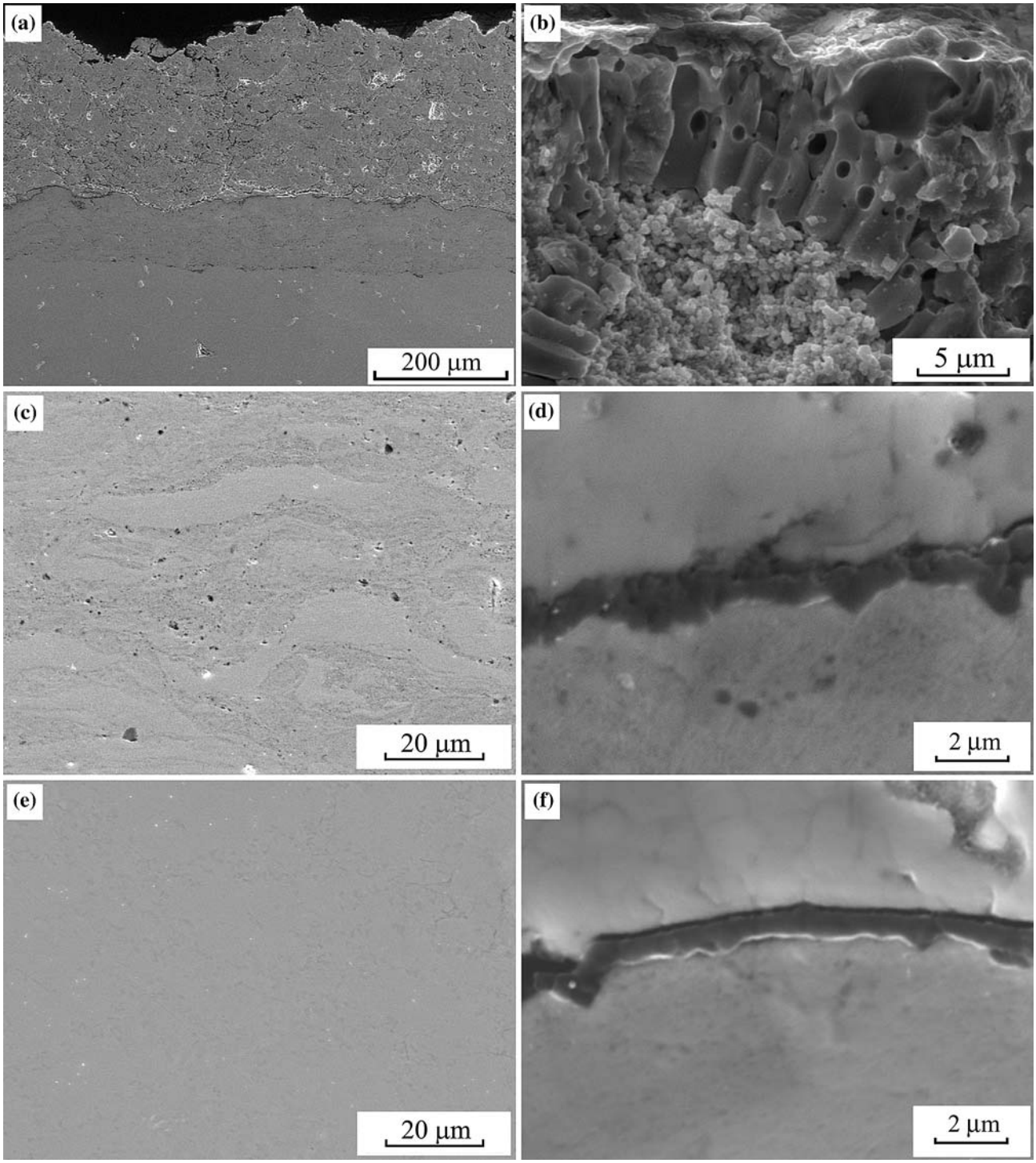

Fig. 2 Cross-sectional microstructure of intact TBCs with nanostructured NiCrAlY/nanostructured YSZ (a); fractured surface of nanostructured YSZ in the TBCs (b); microstructure of nanostructured bond coat (c); typical morphology of TGO formed on the nanostructured bond coat prior to YSZ deposition (d); microstructure of conventional bond coat (e); and typical morphology of TGO formed on the conventional bond coat (f)

1000 °C for 100 h. Two nanostructured TBCs samples withstood further 38 and 36 thermal cycles at 1150 °C, respectively. The failure of the coatings in two nanostructured TBC samples occurred within the topcoat through spalling of YSZ within YSZ coating close to the YSZ/thermal growth oxide interface. The failed cross-sectional microstructure of the conventional TBCs was shown in Fig. 8. It was noted that the failure also occurred

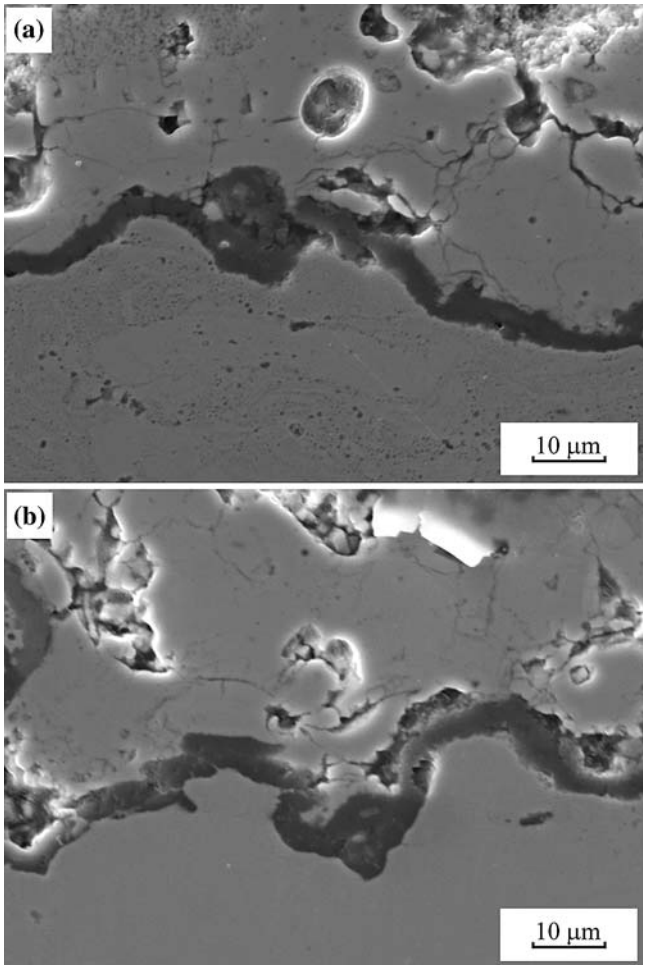

Fig. 3 Cross-sectional microstructure of nanostructured TBCs (a) and conventional TBCs (b) after the isothermal oxidation for 100 h at 1000 °C

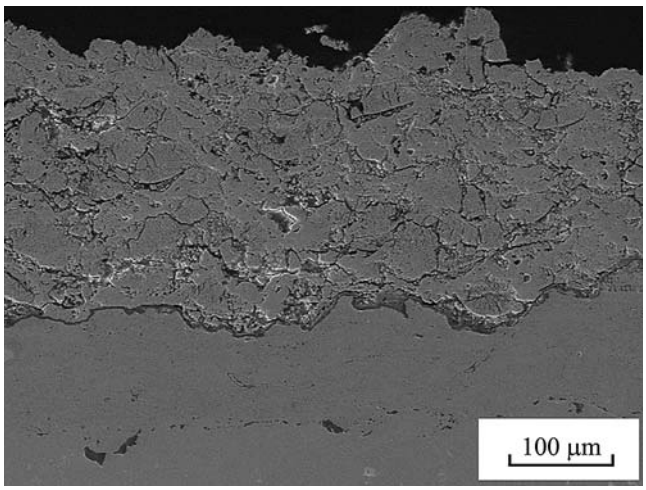

Fig. 4 Cross-sectional micrograph of nanostructured TBCs after thermal cyclic test for 300 cycles at 1000 °C

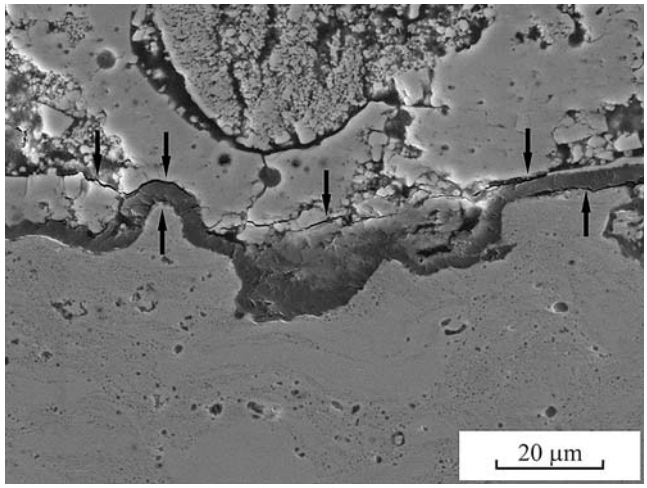

Fig. 5 Cross-sectional micrograph of nanostructured TBCs showing crack formed in the vicinity of the TGO after thermal cyclic test for 300 cycles at 1000 °C

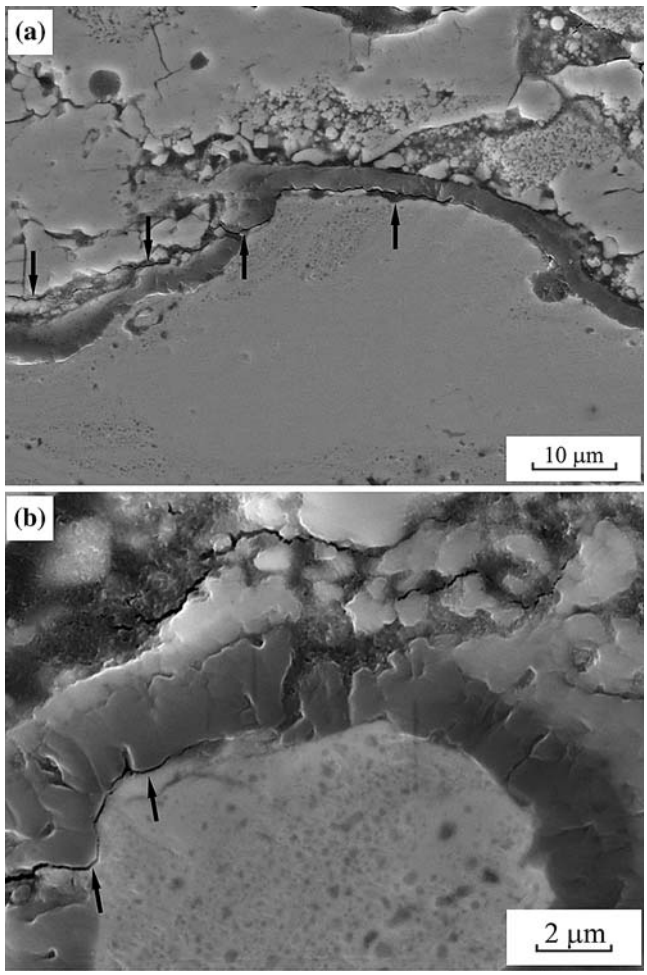

Fig. 6 Cross-sectional micrograph of nanostructured TBCs showing crack formed near the crest after thermal cyclic test for 300 cycles at 1000 °C. (a) and (b) taken by different zone

Table 1 Thermal cycles of the nanostructured and conventional TBCs

Type:	Nanostructured TBCs						Conventional TBCs					
Pretreatment:	1000 °C × 300 cycles			1000 °C × 100 h			1000 °C × 300 cycles			1000 °C × 100 h		
Life	19	38	38	23	36	45	7	10	10	24	29	35
Mean life	32			34			9			29		

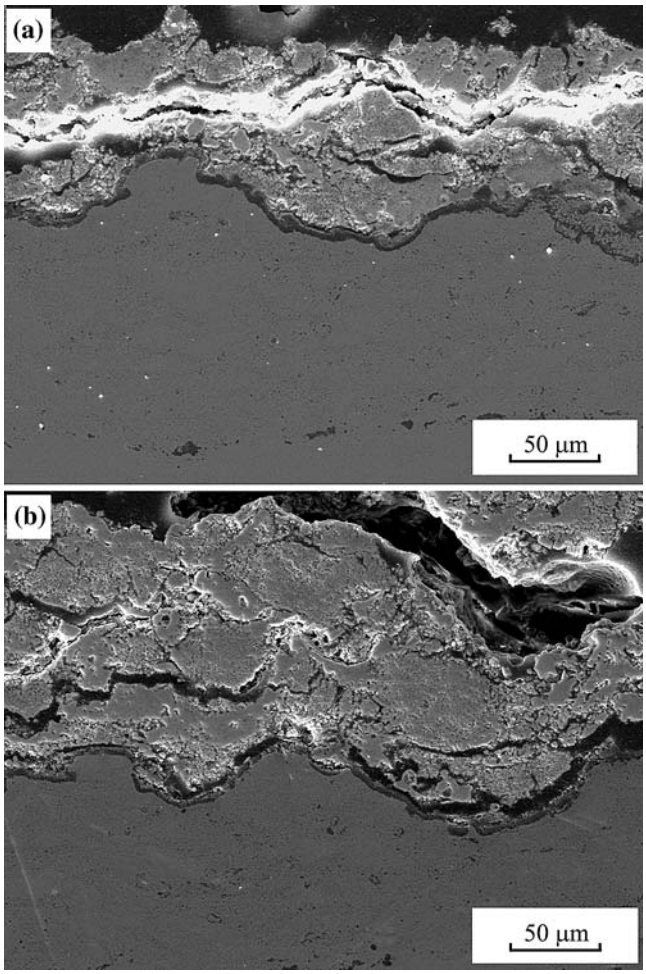

Fig. 7 Cross-sectional micrograph of the failed nanostructured TBCs. (a) The sample experienced 38 cycles at 1150 °C after 300 cycles at 1000 °C; (b) the sample experienced 36 cycles at 1150 °C after isothermal oxidation for 100 h at 1000 °C

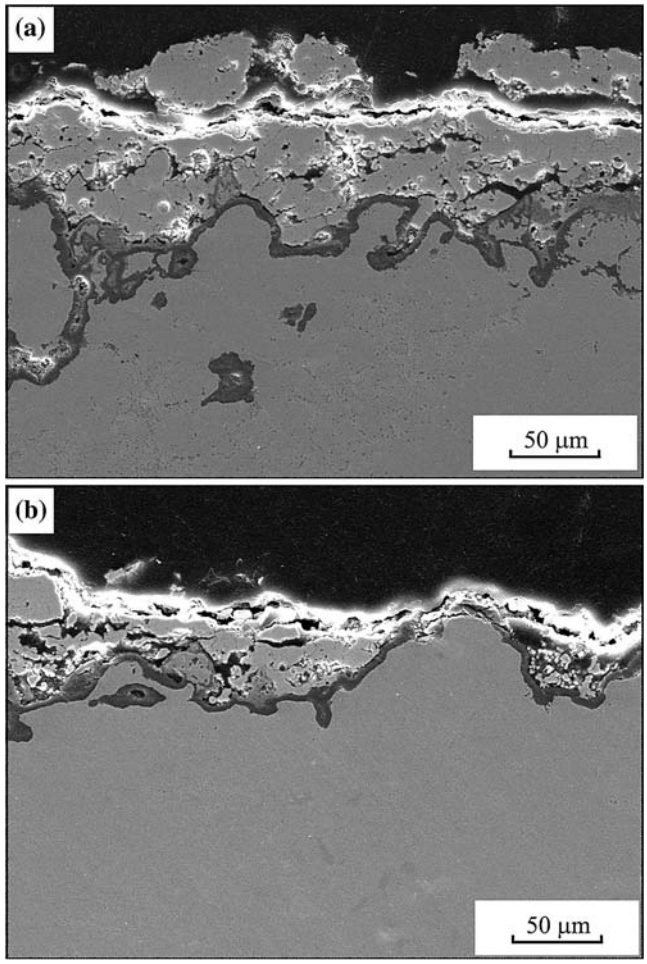

Fig. 8 Cross-sectional micrographs of the failed conventional TBCs. The sample experienced 29 cycles at 1150 °C after isothermal oxidation for 100 h at 1000 °C. (a) and (b) taken by different zone in the failed interface

within the topcoat above TGO, which indicates that the failure of the nanostructured TBCs is similar to the failure scenario of the conventional TBCs (Ref 3-5). However, it was found that the TGO adheres well to the underlying bond coat. Possibly, such well-adhered TGO is attributed to the nanostructure of the bond coat, which promotes the rapid formation of a uniform Al_2O_3 scale on the bond coat surface during the pre-heat treatment (Ref 20-24). Moreover, it was observed in Fig. 9 that the buckling of the nanostructured YSZ topcoat occurred before it spalled out. The buckling may suggest the possibly sealing of YSZ

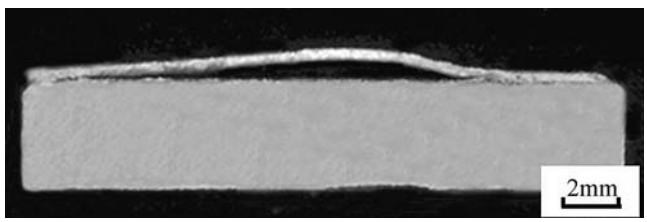

Fig. 9 Cross-sectional micrograph of the failed nanostructured TBCs showing the overview of a buckle. The samples experienced 36 cycles at 1150 °C after isothermal oxidation for 100 h at 1000 °C

topcoat surface through sintering. Although the failure mechanism of the TBC deposited by nanostructured YSZ in the present study is not yet clear, therefore, possibly the sintering of the nanosized YSZ fraction in the coating during high-temperature cyclic test is responsible for the failure of top YSZ coat (Ref 8, 25). This effect is possibly associated with the influence of the thermal cycling at 1000 °C on the thermal shock life of two different TBCs owing to much less sintering and possibly sustainable higher strain tolerability of the nanostructured TBCs. Further detailed study is necessary to reveal the influence of sintering effect and strain tolerability on the thermal failure of the nanostructured TBCs and different failure behavior of two types of the TBCs.

4. Conclusions

Nanostructured YSZ coating was deposited by partially melted YSZ particles. The nonmelted fraction of spray particles retained the porous nanostructure of the starting powder into the deposit. As a result, the nanostructured YSZ coating exhibits a bimodal microstructure consisting of nanosized particles retained from the powder and microcolumnar grains formed through the solidification of the melted fraction in spray particles. The oxidation of the cold-sprayed nanostructured and conventional NiCrAlY bond coat occurred during the heat treatment in Ar atmosphere, and the denser oxides were formed on the nanostructured NiCrAlY bond coat compared with the conventional bond coat. The uniform oxide can be formed during isothermal test at the interface between the bond coat and YSZ in two different TBCs. On the other hand, the cracks were observed at the interface between TGO/BC or TGO/YSZ after thermal cyclic test. However, the failure of both TBCs mainly occurred within the ceramic TBC near the ceramic/TGO coating interface through spalling of YSZ within YSZ coating. Nanostructured thermal barrier coatings exhibits relatively longer lifetime than the conventional coating at cyclic testing at 1150 °C.

Acknowledgments

The present work is supported by National Basic Research Program (Grant No. 2007CB707702), National Science Fund for Distinguished Young Scholars (Grant No. 50725101), and Research Foundation of National Key Laboratory for High Energy Density Beam Processing Technology (Grant No. 51461070705JW0805).

References

1. A.G. Evans, D.R. Mumm, J.W. Hutchinson, G.H. Meier, and F.S. Pettit, Mechanisms Controlling Durability of Thermal Barrier Coating, *Prog. Mater. Sci.*, 2001, **46**(5), p 505-553
2. N.P. Padture, M. Gell, and E.H. Jordan, Thermal Barrier Coatings for Gas-Turbine Engine Applications, *Science*, 2002, **296**, p 280-284
3. K.W. Schlichting, N.P. Padture, E.H. Jordan, and M. Gell, Failure Modes in Plasma-Sprayed Thermal Barrier Coatings, *Mater. Sci. Eng. A*, 2003, **342**(1-2), p 120-130
4. A. Rabiei and A.G. Evans, Failure Mechanisms Associated with the Thermally Grown Oxide in Plasma-Sprayed Thermal Barrier Coatings, *Acta Mater.*, 2000, **48**(15), p 3963-3976
5. E.P. Busso, J. Lin, and S. Sakurai, A Mechanistic Study of Oxidation-Induced Degradation in a Plasma-Sprayed Thermal Barrier Coating System: Part II: Life Prediction Model, *Acta Mater.*, 2001, **49**(9), p 1529-1536
6. C.G. Zhou, N. Wang, Z.B. Wang, S.K. Gong, and H.B. Xu, Thermal Cycling Life and Thermal Diffusivity of a Plasma-Sprayed Nanostructured Thermal Barrier Coating, *Scr. Mater.*, 2004, **51**(10), p 945-948
7. C.G. Zhou, N. Wang, and H.B. Xu, Comparison of Thermal Cycling Behavior Plasma-Sprayed Nanostructured and Traditional Thermal Barrier Coatings, *Mater. Sci. Eng. A*, 2007, **452-453**, p 569-574
8. R.S. Lima and B.R. Marple, Nanostructured YSZ Thermal Barrier Coatings Engineered to Counteract Sintering Effects, *Mater. Sci. Eng. A*, 2008, **485**(1-2), p 182-193
9. R.S. Lima, A. Kucuk, and C.C. Berndt, Integrity of Nanostructured Partially Stabilized Zirconia after Plasma Spray Processing, *Mater. Sci. Eng. A*, 2001, **313**(1-2), p 75-82
10. B. Liang and C.X. Ding, Thermal Shock Resistances of Nanostructured and Conventional Zirconia Coatings Deposited by Atmospheric Plasma Spraying, *Surf. Coat. Technol.*, 2005, **197**(1), p 185-192
11. C.X. Zhang, C.G. Zhou, H. Peng, S.K. Gong, and H.B. Xu, Influence of Thermal Shock on Insulation Effect of Nano-multilayer Thermal Barrier Coatings, *Surf. Coat. Technol.*, 2007, **201**(14), p 6340-6344
12. W.Q. Wang, C.K. Sha, D.Q. Sun, and X.Y. Gu, Microstructural Feature, Thermal Shock Resistance and Isothermal Oxidation Resistance of Nanostructured Zirconia Coating, *Mater. Sci. Eng. A*, 2006, **424**(1-2), p 1-5
13. Q. Zhang, C.J. Li, C.X. Li, G.J. Yang, and S.C. Lui, Study of Oxidation Behavior of Nanostructured NiCrAlY Bond Coatings Deposited by Cold Spraying, *Surf. Coat. Technol.*, 2008, **202**(14), p 3378-3384
14. R.S. Lima, A. Kucuk, and C.C. Berndt, Evaluation of Microhardness and Elastic Modulus of Thermally Sprayed Nanostructured Zirconia Coatings, *Surf. Coat. Technol.*, 2001, **135**(2-3), p 166-172
15. J. Karthikeyan, C.C. Berndt, J. Tikkanen, S. Reddy, and H. Herman, Plasma Spray Synthesis of Nanomaterial Powders and Deposits, *Mater. Sci. Eng. A*, 1997, **238**(2), p 275-286
16. R.S. Lima, A. Kucuk, and C.C. Berndt, Bimodal Distribution of Mechanical Properties on Plasma Sprayed Nanostructured Partially Stabilized Zirconia, *Mater. Sci. Eng. A*, 2002, **327**(2), p 224-232
17. Z.Y. Liu, W. Gao, K.L. Dahm, and F.H. Wang, Improved Oxide Spallation Resistance of Microcrystalline Ni-Cr-Al Coating, *Oxid. Met.*, 1998, **50**(1-2), p 51-69
18. L. Ajdelstajn, F. Tang, G.E. Kim, V. Provenzano, and J.M. Schoenung, Synthesis and Oxidation Behavior of Nanocrystalline MCrAlY Bond Coatings, *J. Therm. Spray Technol.*, 2005, **14**(1), p 23-30
19. D. Toma, W. Brandl, and U. Köster, The Characteristics of Alumina Scales Formed on HVOF-Sprayed MCrAlY Coatings, *Oxid. Met.*, 2000, **53**(1), p 125-137
20. H. Lau, C. Leyens, U. Schulz, and C. Friedrich, Influence of Bond Coat Pre-Treatment and Surface Topology on the Lifetime of EB-PVD TBCs, *Surf. Coat. Technol.*, 2003, **165**(3), p 217-223
21. M. Matsumoto, T. Kato, K. Hayakawa, N. Yamaguchi, S. Kitaoka, and H. Matsubara, The Effect of Pre-Oxidation Atmosphere on the Durability of EB-PVD Thermal Barrier Coatings with CoNiCrAlY Bond Coats, *Surf. Coat. Technol.*, 2008, **202**(12), p 2743-2748
22. R. Darolia, Post-Deposition Oxidation of a Nickel-Base Superalloy Protected by a Thermal Barrier Coating, US Patent 6,607,611, 19 August 2003

23. M.J. Weimer, B.A. Nagaraj, A. Bangalore, J.C. Schaeffer, and J.A. Heaney, Pre-Service Oxidation of Gas Turbine Disk and Seal, US Patent 6,532,657, 18 March 2003
24. T.J. Nijdam, L.P.H. Jeurgens, J.H. Chen, and W.G. Sloof, On the Microstructure of the Initial Oxide Grown by Controlled Annealing and Oxidation on a NiCoCrAlY Bond Coating, *Oxid. Met.*, 2005, **64**(5-6), p 355-377
25. O. Racek, C.C. Berndt, D.N. Guru, and J. Heberlein, Nanostructured and Conventional YSZ Coatings Deposited Using APS and TTPR Techniques, *Surf. Coat. Technol.*, 2006, **201**(1-2), p 338-346